Universiteit
Leiden
The Netherlands

Ruthenium– and cobalt–based artificial metalloenzymes for photocatalytic water oxidation in artificial photosynthesis

Polanco Rivas, E.A.

Citation

Polanco Rivas, E. A. (2023, June 7). *Ruthenium– and cobalt–based artificial metalloenzymes for photocatalytic water oxidation in artificial photosynthesis*. Retrieved from https://hdl.handle.net/1887/3619951

Version:	Publisher's Version
License:	Licence agreement concerning inclusion of doctoral thesis in the Institutional Repository of the University of Leiden
Downloaded from:	https://hdl.handle.net/1887/3619951

Note: To cite this publication please use the final published version (if applicable).

Chapter 5

Protein-protein interaction for photocatalytic water oxidation

This chapter will be *submitted* for publication: A*rtificial Protein-protein interaction for water oxidation for water oxidation.* Polanco E.A.; Stinger, L.; Opdam, L.V.; Bonnet, S.; Pandit, A. (*in preparation*)

5.1 Introduction

Protein-protein interactions (PPIs) are crucial for biological processes such as cell signalling, respiration,[1–3] or drug delivery. Many research groups focus on PPIs to also understand the electron transfer pathways in enzymatic complexes such as photosystem II (PSII, Figure 5.1).[4–6] A challenging requirement to mimic the photosynthetic process is to have highly active catalytic centres in a supramolecular system capable of promoting charge separation and unidirectional electron transfer, while slowing down charge recombination. In natural photosynthesis, these active centres have found a fixed position in the cell membrane using interacting proteins, which altogether tightly regulates the efficacy and directionality of the electron transfer processes.[7] Minimum models capable of mimicking this complex enzymatic system have been developed, where a metal complexes (*i.e.* based on Ru, Re, Co or Ir) capable of driving the O_2 evolution, H_2 evolution, or CO_2 reduction, were supported at a liposome surface together with light-absorbing photosensitizers.[8–10] An alternative approach is to use artificial metalloenzymes, in which a catalytically active metal complex is attached to a protein backbone.[11] Recent reports have shown that fixing an active H_2 evolution catalyst to a protein such as hydrogenase or myoglobin generates an environment around the catalyst that increases its activity, compared to the protein-free metal catalyst.[12–14] However, assembling a biomimetic PSII analogue would require to connect such ArMs to light-absorbing systems, and to manage electron and proton transfer through a membrane.[15] This have been accomplished labelling proteins using luminescent dyes which has allowed to prove electron transfer, protein-ligand, or PPI.[16–18] Some of these systems involve wild-type proteins fixed at an electrode surface and performing catalysis in electrochemical conditions.[19–22] Up to now, reports on artificial metalloenzymes for artificial photosynthesis have been scarce.[23,24] Herein, we describe the study of PPIs between two ruthenium-based artificial metalloenzymes: one capable of acting as photosensiziter, noted **BSA-Ru$_{PS}$**, and a second one capable of driving the water

oxidation reaction, noted **BCA-Ru$_{WOC}$** (Figure 5.1). Together, they form one of the rare functional models of PSII capable of photocatalytic water oxidation.

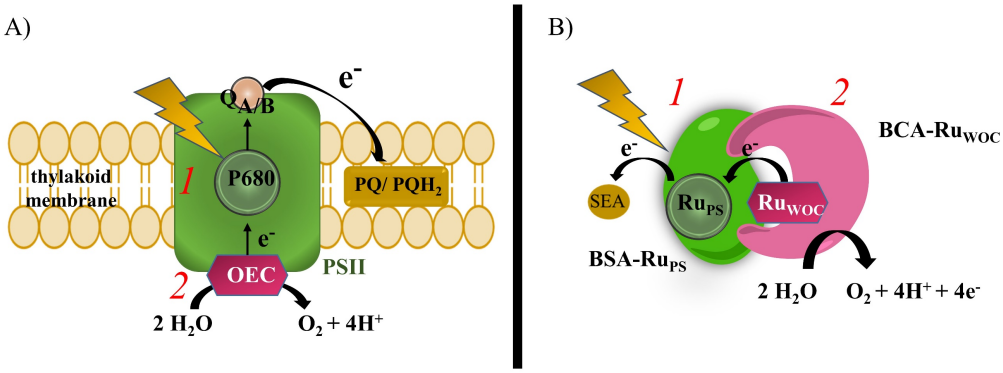

Figure 5.1. (**A**) Schematic representation of the two characteristic sites of the PSII charge-separating unit, composed of a photosensitizer, P680, and an oxygen-evolving catalytic center, noted OEC. Both are inserted in the thylakoid membrane. (**B**) Cartoon representation of the artificial system presented in this work as a mimic of the two main elements of PSII interacting *via* PPI: **BSA-Ru$_{PS}$** as an artificial P680, and **BCA-Ru$_{WOC}$** as artificial OEC. **Ru$_{PS}$** and **Ru$_{WOC}$** represent both artificial cofactors bound to the two protein scaffolds.

5.2 Results

5.2.1. A ruthenium-BSA artificial light-harvesting protein

First, an artificial ruthenium-based protein was prepared to function as a charge separating molecule for photocatalytic water oxidation. For this purpose, we covalently coupled the classical $[Ru^{II}(bpy)_3]^{2+}$ photosensitizer (PS) to Bovine serum albumin (**BSA**), which was used as protein scaffold. To realise the coupling, we used the free Cys34 residue, which is located in an accessible position at the protein surface, and a $[Ru(bpy)_3]^{2+}$ functionalized with a maleimide group, noted **Ru$_{PS}$** (Figure 5.2), which was proven to react selectively to Cys residues.[25–27] A maleimide group was introduced in 5-position on a 1,10-phenanthroline ligand in a two-step synthesis (Figure AIV.1). Then, the ligand was coordinated to $[Ru(bpy)_2Cl_2]$ affording **Ru$_{PS}$**.[28] The main advantage of this strategy is that it allows for conjugating

a single equivalent of **Ru$_{PS}$** per protein unit, since only one cysteine position (Cys34) on the protein backbone is available for covalent binding of **Ru$_{PS}$** to **BSA.**

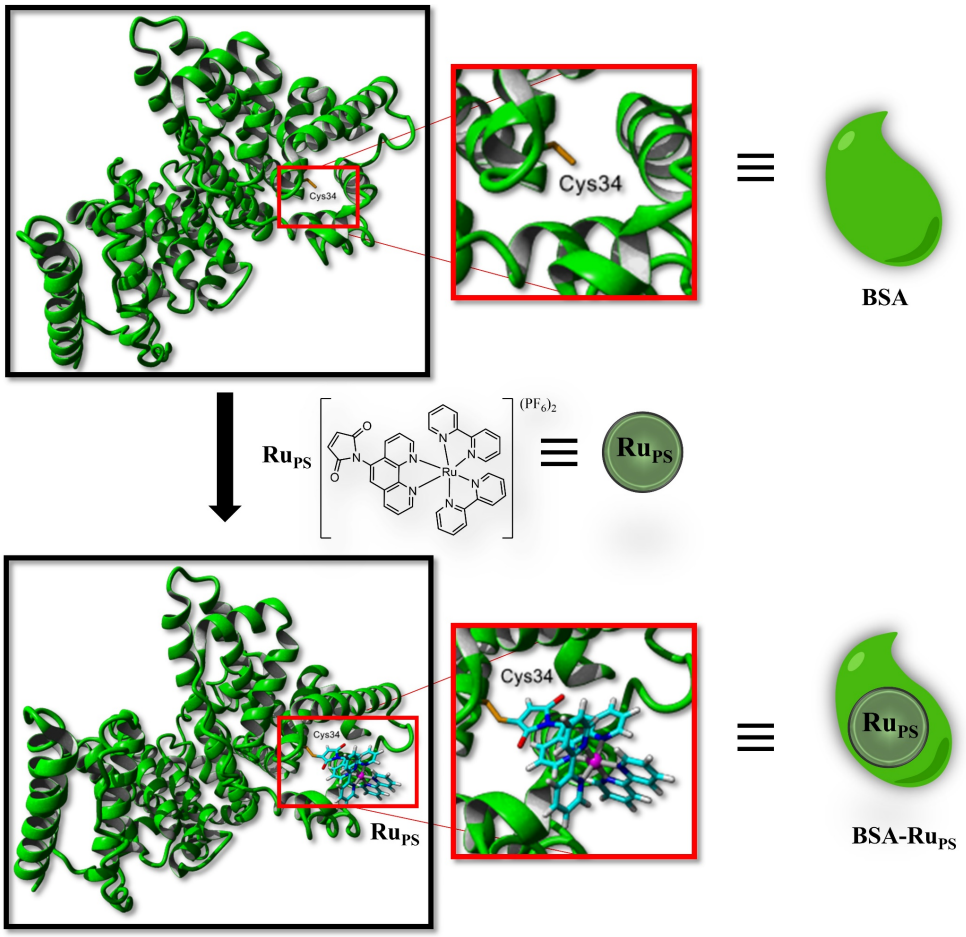

Figure 5.2. Representation of **BSA** and of the free cysteine residue Cys34 used for covalent functionalization of the protein with **Ru$_{PS}$**. The protein scaffold (green) and Cys34 residue (orange) were obtained from PDB *3V03*. Conditions**:** phosphate buffer pH 7.0 (20 mM), temperature 4 °C, overnight, dark, [**BSA**] = 0.2 mM, [**Ru$_{PS}$**] = 2 mM (dissolved in DMF), Ratio protein:complex 1:10.

The functionalization of **BSA** with **Ru$_{PS}$** to produce the artificial light-scavenger protein **BSA-Ru$_{PS}$** consisted in incubating **BSA** with an excess (10 eq.) **Ru$_{PS}$** to ensure all Cys34 residues were bound to **Ru$_{PS}$** (Figure 5.2). In addition, the reaction

was performed at neutral pH (pH 7.0) to promote only the interaction between **Ru$_{PS}$** and Cys34 of **BSA**, and not with any other residues such as lysine, which when unprotonated might also react with the maleimide group at basic pH for example.[29] After 12 h incubation the excess **Ru$_{PS}$** was removed using a desalting Bio-Rad column. The complex-protein binding was analysed using a 7.5 % acrylamide semi-native SDS (Figure 5.3A). The gel showed a new band at higher molecular weight (Lanes: 1, 2 and 3, triplicate) compared to free **BSA** (Lane: **BSA**). A very illustrative way to directly observe the complex-protein interaction was to place the eluted gel under a 254 nm UV light: orange phosphorescence was observed for the new band, which is characteristic for phosphorescence emission by $[Ru(bpy)_3]^{2+}$, while nothing was visible for the bands corresponding to free **BSA**. Further, ESI-MS analysis showed signals corresponding to the adduct **[BSA-Ru$_{PS}$ + H$_2$O]** (67122 Da, Figure AIV.4). Circular dichroism (CD) was used to see if the binding of **Ru$_{PS}$** generated a significant change of the protein conformation (Figure 5.3B). The spectrum of free **BSA** was in fact very similar to that of the artificial protein **BSA-Ru$_{PS}$**. These results demostrated that **Ru$_{PS}$** not only binds to free **BSA** in the conditions studied to produce an artificial visible light-absorbing protein, **BSA-Ru$_{PS}$** but also that upon doing so it did not change the conformation of the protein itself.

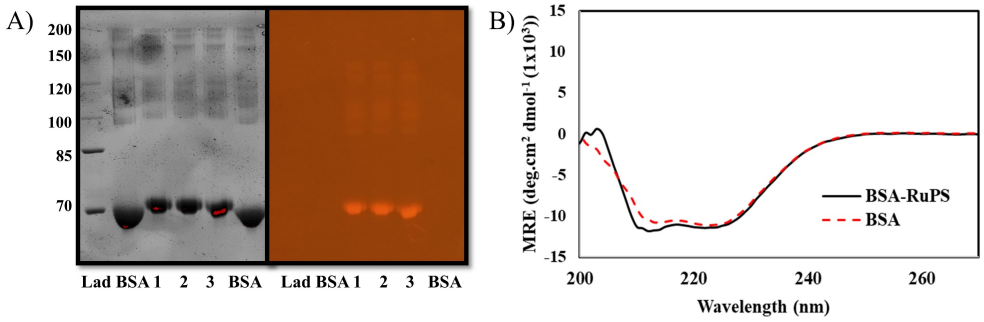

Figure 5.3. 7.5 % polyacrylamide semi-native SDS gel of **BSA** covalently functionalized with **Ru$_{PS}$** (**A**) (*left* normal gel *(right)* gel under UV light (254 nm). Lanes: Lad = protein ladder, **BSA** = free **BSA**, 1, 2 and 3 = **BSA-Ru$_{PS}$** (triplicate). (**B**) CD spectra of free **BSA** (dotted line) and **BSA-Ru$_{PS}$** (straight

line). [**BSA**] = [**BSA-Ru$_{PS}$**] = 10 μM, phosphate buffer pH 7.5 (80 mM). Mean residue ellipticity (MRE) was calculated according literature.[30]

The effects of the covalent attachment to the **BSA** scaffold on the photochemical properties of **Ru$_{PS}$** in the artificial **BSA-Ru$_{PS}$** protein were analysed via various spectroscopic techniques. First, the absorption and emission spectra of **BSA-Ru$_{PS}$** were recorded (Figure 5.4A). The absorbance was characterized by a maximum (λ_{abs}^{max}) at 455 nm, and the emission maxima (λ_{em}^{max}) was found at 604 nm, which are both similar to those of free $[Ru(bpy)_3]^{2+}$ in similar conditions. However, in similar conditions the emission intensity of free $[Ru(bpy)_3]^{2+}$ was found to be higher than that of **BSA-Ru$_{PS}$** (Figure AIV.5), suggesting some form of quenching. Second, quenching of the ruthenium emission by the sodium persulfate electron acceptor[31] was studied by steady-state emission spectroscopy. The phosphorescence emission at 604 nm was quenched by increasing concentrations of sodium persulfate (Figure 5.4B). The corresponding Stern-Volmer plot gave a K_{SV} value of 0.37 (Figure 5.4C) and the lifetime of the excited specie ^{3}[**BSA-Ru$_{PS}$**]$^{2+\bullet}$ was long (τ^0 = 0.73 μs), as expected for a triplet excited state. In comparison with free $[Ru(bpy)_3]^{2+}$ in similar conditions (τ^0 = 0.32 μs, K_{SV} = 15:1, Figure AIV.6), the protein scaffold appeared to slightly increase the lifetime of the triplet excited state, while the Stern-Volmer constant K_{SV} was significantly lowered. From these values, the second-order quenching rate constant, k_q, was 0.5 and 40 $M^{-1}s^{-1}$ for **BSA-Ru$_{PS}$** and free $[Ru(bpy)_3]^{2+}$, respectively, which highlight the slower diffusion of the sensitizer once bound to the large protein molecule. Finally, the photostability of the **BSA-Ru$_{PS}$** conjugate was studied by following its UV-vis spectrum under blue light irradiation (450 nm) in phosphate buffer pH 7.5 (Figure 5.4D). The visible part of the spectrum remained constant but the UV absorption increased once the samples started to be irradiated. To analyse further what happened, three blanks experiments were performed: 1) Irradiation of free **BSA**, 2) Irradiation of free $[Ru(bpy)_3]^{2+}$ and 3) irradiation of a 1:1 **BSA**: $[Ru(bpy)_3]^{2+}$ mixture (Figure AIV.6). No changes in the

UV region for the samples containing free **BSA** or free $[Ru(bpy)_3]^{2+}$ were observed. However, for the sample containing the 1:1 **BSA**: $[Ru(bpy)_3]^{2+}$ mixture a similar, though slower evolution of the UV part of the spectrum, was observed. These results demonstrated the binding of **Ru$_{PS}$** to the **BSA** scaffold, which produced a light-sensitive protein with light-harvesting properties, **BSA-Ru$_{PS}$**.

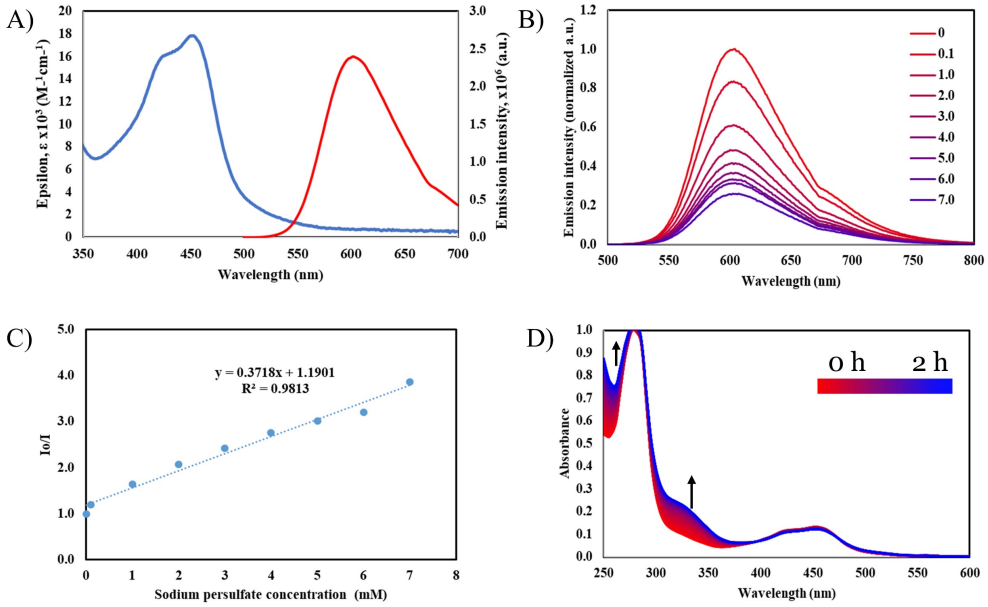

Figure 5.4. (**A**) Absorption (blue, left) and emission (red, right) spectra of **BSA-Ru$_{PS}$**. Conditions: [**BSA-Ru$_{PS}$**] = 20 μM, phosphate buffer pH 7.5 (80 mM), excitation at 450 nm. (**B**) Emission quenching of **BSA-Ru$_{PS}$** with increasing concentrations of sodium persulfate ($Na_2S_2O_8$, 0-7 mM). (**C**) Stern-Volmer plot of **BSA-Ru$_{PS}$** quenched by sodium persulfate ($Na_2S_2O_8$). Conditions: [**BSA-Ru$_{PS}$**] = 20 μM, [$Na_2S_2O_8$] = 0 to 7 mM, phosphate buffer pH 7.5 (80 mM), excitation at 450 nm. (**D**) Evolution of the UV-vis spectrum of **BSA-Ru$_{PS}$** under blue light irradiation. Conditions: [**BSA-Ru$_{PS}$**] = 10 μM, 450 nm (18 mW), 25 ºC, phosphate buffer pH 7.5 (80 mM).

5.2.2. O_2 evolution with artificial proteins: an artificial PSII

In Chapter 4, we reported an artificial enzyme constructed from carbonic anhydrase and a ruthenium 6,6'-biscarboxylatobipyridine, **BCA-Ru1**, that was capable to catalyse water oxidation in photocatalytic conditions. Here, we mixed **BCA-Ru1** and the photosensitizer **BSA-Ru$_{PS}$** to study the capacity of the resulting

artificial protein-based system to promote the O_2 evolution reaction (OER) under blue light irradiation, using sodium persulfate as sacrificial electron acceptor (SEA). Henceforth, **BCA-Ru1** will be re-labelled as **BCA-Ru$_{WOC}$**. As shown in Figure 5.5 (pink trace), the artificial protein **BCA-Ru$_{WOC}$** (5 μM) was inactive in absence of photosensitizer in the dark, showing there was no dark catalytic water oxidation driven by peroxodisulfate. Nevertheless, when $[Ru(bpy)_3]^{2+}$ was used as photosensitizer and was exposed to blue light for 120 min, **BCA-Ru$_{WOC}$** was active for water oxidation, producing ~4 μmol O_2 (blue trace). When the free photosensitizer was replaced by the artificial light-harvesting protein **BSA-Ru$_{PS}$** the system under light irradiation showed a comparable activity to the previous system, producing ~3 μmol of O_2 in 120 min (red). In this experiment, a much lower concentration of photosensitizer was needed (**BSA-Ru$_{PS}$** = 20 μM), compared to that used for the experiment with free $[Ru(bpy)_3]^{2+}$, which required 300 μM photosensitizer. To compare the effect of **BSA** host of the photosensitizer **Ru$_{PS}$**, the photocatalysis was performed using the same concentration of **BCA-Ru$_{WOC}$** (5 μM) but a 20 μM concentration of free photosensitizer $[Ru(bpy)_3]^{2+}$ (grey trace): in such conditions O_2 evolution was lower (~0.5 μmol) than when using 20 μM **BSA-Ru$_{PS}$**. These results showed that **BSA-Ru$_{PS}$** was a much better photosensitizer for this system than $[Ru(bpy)_3]^{2+}$, leading to the suggestion that a protein–protein interaction may take place between the two artificial proteins. This interaction might allow to promote water oxidation at the low photosensitizer concentrations of the photocatalytic system studied here.

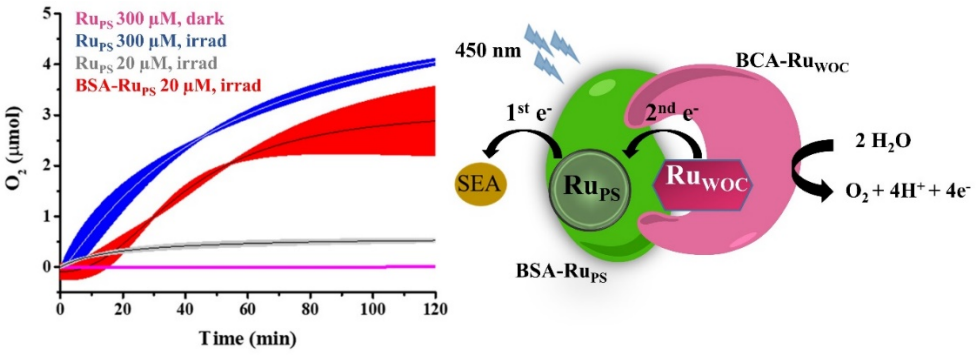

Figure 5.5. (**A**) O_2 evolution when a mixture of **BCA-Ru$_{WOC}$**, **[Ru(bpy)$_3$](ClO$_4$)$_2$** or **BCA-Ru$_{PS}$**, and $Na_2S_2O_8$, were stirred in the dark (pink), or under light irradiation. Blue trace: **[Ru(bpy)$_3$](ClO$_4$)$_2$** concentration = 300 µM; grey trace: **[Ru(bpy)$_3$](ClO$_4$)$_2$** concentration = 20 µM. Red trace: **BCA-Ru$_{PS}$** concentration = 20 µM. Conditions: total volume 3.5 mL, excitation wavelength 450 nm , 19 mW, temperature 25 °C; phosphate buffer pH 7.5 (80 mM), SEA: [$Na_2S_2O_8$] = 2 mM, [**BCA-Ru$_{WOC}$**] = 5 µM. Irradiation started at t = 0 min. Data fitted in OriginPro using Hill function. The black lines (white for blue trace) represent averages over 2 independent measurements; errors (SD) are represented as coloured bands. For raw data see Figure AIV.8. (**B**) Representation of PPI for O_2 evolution under light irradiation in presence of SEA.

5.2.3 Studying the interaction between BSA- Ru$_{PS}$ and BCA-Ru$_{WOC}$

In order to check this hypothesis, SDS-page gel electrophoresis was first used to monitor the interaction between the artificial proteins **BSA-Ru$_{PS}$** and **BCA-Ru$_{WOC}$**. As shown in Figure 5.6A, the gel showed a striking difference before and after 120 min photocatalysis. After photocatalysis (Lane 4) the bands corresponding to **BSA-Ru$_{PS}$** were no longer visible, but a higher band at the top of the gel had formed. We hypothesize that this new band at higher molecular weight (>200 kDa) may correspond to an aggregated or cross-linked species formed during light irradiation of the two proteins.[32,33] To prove this, we studied the protein system in presence or in absence of the free ruthenium complexes (Figure 5.6B). Initially, we irradiated a sample containing **BSA-Ru$_{PS}$** and **BCA-Ru$_{WOC}$** in absence of sodium persulfate. Upon irradiation, the band corresponding to **BSA-Ru$_{PS}$** was not longer traceable but a smear band with no clear appareance of higher molecular weight

was detected (Lane 6 and 7). Afterwards, using blue light we irradiated samples containing **BSA-Ru$_{PS}$** and **Ru$_{WOC}$** in presence of sodium persulfate (Lane 8 and 9). After 2 h irradiation, the band corresponding to **BSA-Ru$_{PS}$** disappeared and a smear but no band at higher molecular weight as well. Then, we irradiated samples containing free **BSA** and free **BCA** (no complex bound) in absence and in presence of $[Ru(bpy)_3](ClO_4)_2$ (Figure 5.6C). When the photosensitizer was absent, no changes in the SDS-page took place, which showed the same bands after 2 h irradiation as before (Lane 10 and 11). In addition, when **BSA** was irradiated in presence of **BCA** and the ruthenium photosensitizer, the band of **BSA** disappeared and a new band at the top of the gel became present (Lane 12 and 13). To confirm the formation of this band was due to the photosensitizer, a sample containing **BSA-Ru$_{PS}$** and free **BCA** catalyst was irradiated, after which the SDS-page showed the formation of the same band at the top of the gel (Lane 14 and 15). Altogether, these results demonstrated that the formation of a high molecular weight specie observed in SDS-page is formed when both artificial proteins, **BSA-Ru$_{PS}$** and **BCA-Ru$_{WOC}$** are present in the sample and due to the presence of SEA and the $[Ru(bpy)_3](ClO_4)_2$ sensitizer free or bound to **BSA** during light irradiation.

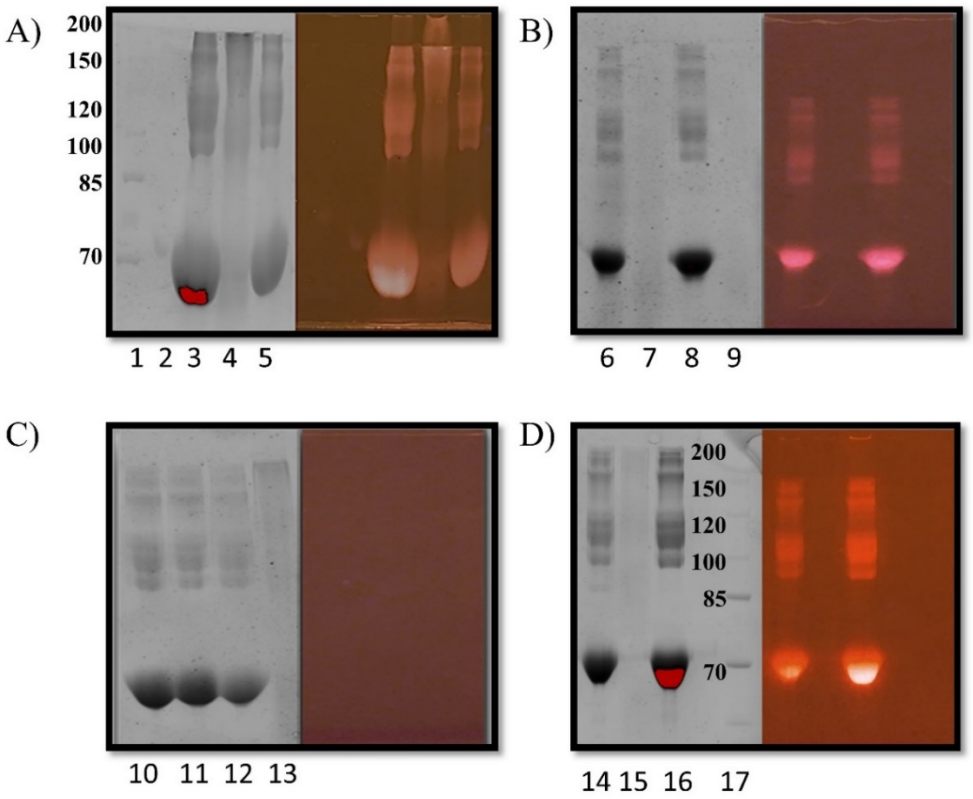

Figure 5.6. 7.5 % polyacrylamide semi-native SDS-page for PPI studies. For each gel image: On the *left* is the picture of the gel taken using the software (See Experimental section) and on the *right* is the picture of the gel placed over a glass under a 254 nm UV-lamp. (**A**) Lane 1: Ladder ; Lane 2: **BCA-Ru$_{WOC}$** dark; Lane 3: **BCA-Ru$_{WOC}$** + **BSA-Ru$_{PS}$** + SEA before irradiation (in the dark); Lane 4: **BCA-Ru$_{WOC}$** + **BSA-Ru$_{PS}$** + SEA after irradiation; Lane 5: **BSA-Ru$_{PS}$** dark. Conditions: [**BCA-Ru$_{WOC}$**] = 5 μM, [**BSA-Ru$_{PS}$**] = 0.3 mM, SEA :[$Na_2S_2O_8$] = 2 mM, 450 nm, temperature 25 °C, phosphate buffer pH 7.5 (80 mM). (**B**) Effect of **BCA** protein scaffold in PPI: Lane 6: **BCA-Ru$_{WOC}$** + **BSA-Ru$_{PS}$** in the dark; Lane 7: **BCA-Ru$_{WOC}$** + **BSA-Ru$_{PS}$** after irradiation; Lane 8: **Ru$_{WOC}$** + **BSA-Ru$_{PS}$** + SEA dark; Lane 9:**Ru$_{WOC}$** + **BSA-Ru$_{PS}$** + SEA after irradiation. (**C**) Effect of the photosensitizer in PPI: Lane 10: **BCA** + **BSA** dark; Lane 11: **BCA** + **BSA** after irradiation; Lane 12: **BCA** + **BSA** + $[Ru(bpy)_3](ClO_4)_2$ + SEA dark; Lane 13: **BCA** + **BSA** + $[Ru(bpy)_3](ClO_4)_2$ + SEA after irradiation. (**D**) Effect of **Ru$_{WOC}$** in PPI: Lane 14: **BCA** + **BSA-Ru$_{PS}$** + SEA dark ; Lane 15: **BCA** + **BSA-Ru$_{PS}$** + SEA after irradiation; Lane 16: **BSA-Ru$_{PS}$** dark; Lane 17: Ladder. Conditions: [**BCA-Ru$_{WOC}$**] = 30 μM, [**Ru$_{WOC}$**] = 30 μM, [**BSA-Ru$_{PS}$**] = 60 μM, $[Ru(bpy)_3(ClO_4)_2]$ = 60 μM, [**BSA**] = 60 μM, SEA:[$Na_2S_2O_8$] = 2 mM, 1 mL sample, 450 nm, temperature 25 °C, phosphate buffer pH 7.5 (80 mM). Samples were degassed during

30 min with Ar before light irradiation. Stirring was set at 400 rpm. For irradiation a PhotoRedoxbox setup was used (See Figure AIV.9).

The interaction between **BCA-Ru$_{WOC}$** and **BSA-Ru$_{PS}$** was also studied by absorption spectroscopy. The evolution of the UV-vis spectrum of a solution containing **BCA-Ru$_{WOC}$**, **BSA-Ru$_{PS}$** and sodium persulfate irradiated with blue light for 2 h was recorded (Figure 5.7C). After irradiation, a band at 680 nm was formed. We attributed this band to the formation of a Ru^{3+} specie as result of photocatalytic water oxidation.[34,35] Two control experiments were performed: **BSA-Ru$_{PS}$** and sodium persulfate were first irradiated in absence of **BCA-Ru$_{WOC}$**, and then **BCA-Ru$_{WOC}$** and sodium persulfate were irradiated in absence of **BSA-Ru$_{PS}$** (Figure 5.7A-B). For the first experiment, the spectrum clearly showed depletion of the metal-to-ligand charge transfer (MLCT) absorption band at 450 nm of the ruthenium(II) polypyridyl complex, suggesting the formation of an oxidized ruthenium(III) photoproduct, which should absorb near 370 nm.[31,36] This evolution was not observed when **BSA-Ru$_{PS}$** was irradiated in the same conditions but in the absence of quencher. In such conditions no band at 680 nm was observed, showing that this band only formed in presence of both artificial proteins in the irradiated mixture. These results suggested that the formation of this band in the red region of the absorption spectrum must be the consequence of a redox reaction involving the Ru centers of both proteins, and that this reaction can only occur if **BSA-Ru$_{PS}$** and **BCA-Ru$_{WOC}$** are close from each other.

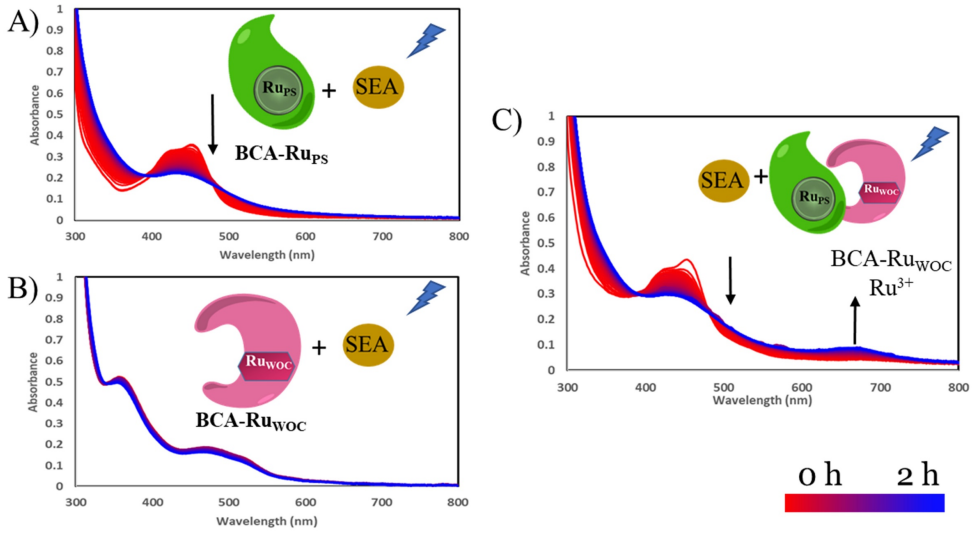

Figure 5.7. UV-vis evolution *vs.* time of the protein-based photocatalytic system. (**A**) **BSA-Ru$_{PS}$** + SEA, (**B**) **BCA-Ru$_{WOC}$** + SEA, and (**C**) **BSA-Ru$_{PS}$** +**BCA-Ru$_{WOC}$** + SEA. **BSA-Ru$_{PS}$** is represented in green, **BCA-Ru$_{WOC}$** is represented in pink and $Na_2S_2O_8$ is represented in yellow. Conditions: [**BCA-Ru$_{WOC}$**] = 5 μM; [**BSA-Ru$_{PS}$**] = 10 μM; SEA = [$Na_2S_2O_8$] = 1 mM; phosphate buffer pH 7.5 (80 mM); temperature 25 ºC; 3.5 mL sample; 450 nm, 19 mW light source.

The probable interaction between **BSA-Ru$_{PS}$** and **BCA-Ru$_{WOC}$** was also studied by DLS to see any potential change in the size distribution of the particles in solution during photocatalysis (Figure AIV.10). The DLS spectra of samples containing **BSA-Ru$_{PS}$**, **BCA-Ru$_{WOC}$** and sodium persulfate were measured before and after 2 h blue light irradiation. In addition, the DLS spectra of each protein **BSA-Ru$_{PS}$** and **BCA-Ru$_{WOC}$** were measured alone as reference. The average particle size from the sample before irradiation (3.3 nm) increased by a factor 0.7 after photocatalysis (4.7 nm). This increment did not match the bands observed in the SDS-gel, which suggested that the protein did not form very large aggregates. In view of this result, the composition of the photocatalytic mixture was analysed by ESI-MS to see if a higher molecular weight protein species was generated (Figure AIV.11). The deconvoluted MS spectrum of the sample of **BSA-Ru$_{PS}$** [20 μM] and **BCA-Ru$_{WOC}$** [5 μM] measured in presence of peroxodisulfate [5 mM] before irradiation showed

the signal of both proteins at 29026 and 67138 Da, respectively. As mentioned in Chapter 4, in the conditions in which ESI-MS analysis was performed, *i.e.,* acidic conditions (presence of formic acid), the adduct **BCA-Ru$_{WOC}$** was unstable, promoting the protonation of the zinc-binding histidines and hence discoordination of the specie Zn^{2+}-Ru$_{WOC}$, making undetectable **BCA-Ru$_{WOC}$** by MS. In contrast, after 2 h light irradiation the spectrum showed signals at 29900 and 70300 Da that were slightly heavier. These signals might originate from the oxidation of the protein residues by O_2 produced during photocatalysis.

CD was then used to study the possible changes of the protein conformation when mixing and irradiating both artificial enzymes. First, the spectrum of a sample containing only **BCA-Ru$_{WOC}$** was recorded as reference (Figure 5.8). The concentration of **BSA-Ru$_{PS}$** was then gradually increased from 0 to 40 μM and the CD spectrum recorded for each concentration. The spectra showed an increased or red-shifted band at ~230 nm and a depletion of the band at 210 nm, which corresponds to the alpha-helical structure of the protein.[37,38] To investigate whether such effects may be due to the ruthenium complexes bound to the proteins (**Ru$_{PS}$** and **Ru$_{WOC}$**), similar experiment was performed using free **BCA** and free **BSA**. The results showed the same depletion of the bands at 210 nm and an increasing band at ~ 230 nm, which could be observed as a red shift of the 220 nm band. The conformation changes upon mixing both proteins seem hence not to be due to the presence of the ruthenium cofactors. This experiment was repeated using a fixed amount of **BSA-Ru$_{PS}$** and increasing the concentration of **BCA-Ru$_{WOC}$**. A more pronounce depletion of the bands at 210 and 220 nm was visible, showing decreased signals related to a denatured protein. The free proteins **BCA** and **BSA** showed the same trend. Overall, **BSA** and **BCA** were found to influence their conformation when put together in a homogeneous aqueous solution, which proves that an interaction occurs between both proteins.

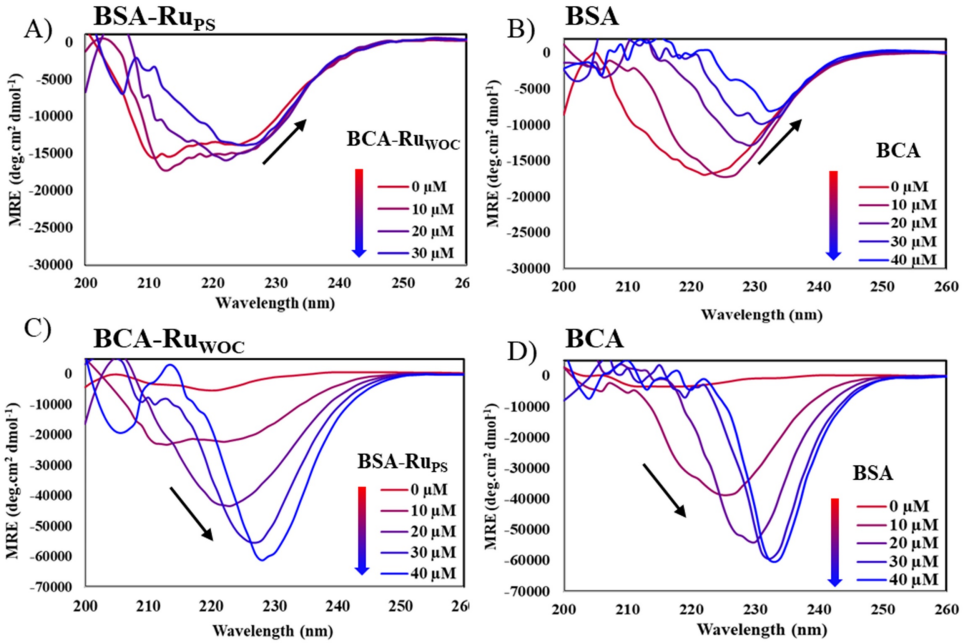

Figure 5.8. Evolution of the CD spectrum of: (**A**) **BSA-Ru$_{PS}$** upon adding **BCA-Ru$_{WOC}$**, (**B**) **BSA** upon adding **BCA**, (**C**) **BCA-Ru$_{WOC}$** upon adding **BSA-Ru$_{PS}$**, (**D**) **BCA** upon adding **BSA**. The concentration of the starting protein was fixed at 10 µM and the concentration of the added protein was increased from 0 to 40 µM (see legend). Conditions: temperature 25 °C, phosphate buffer pH 7.5 (80 mM). Mean residue ellipticity (MRE) was calculated according literature.[30]

5.3. Discussions

Recent research of a system involving **BSA** and carbonic anhydrase (**CA**) showed possible interaction between these protein in biological system.[39–42] However, the role of **BSA** according to these reports is merely a transport of active compounds towards their target, ***i.e.,*** the active site of a specific isozyme of **CA** (**CAIX**) related to tumours development. Currently there is no clear proof of the interaction between these two proteins. So far, the **BCA-BSA** adduct and its possible application for solar energy conversion has not been studied yet.

Here incorporation of a maleimide group in one of the diimine chelates of $[Ru(bpy)_3]^{2+}$ allows for functionalizing **BSA** with **Ru$_{PS}$** to produce a light-absorbing artificial protein, **BSA-Ru$_{PS}$**. The protein scaffold was showed to affect the

properties of the Ru centre as it increased its phosphorescence intensity at 604 nm and its lifetime from 0.3 to 0.7 μs.[43] In addition, the decrease in the quenching rate constant k_q upon conjugation to the protein backbone showed that the electron transfer between the excited specie of the photosensitizer and the quencher, sodium persulfate, is faster for free $[Ru(bpy)_3]^{2+}$ than for the ruthenium sensitizer bound to **BSA**, called **BSA-Ru$_{PS}$**. This effect must be due to the hydrophobic environment provided by the protein around the ruthenium complex. It also shows that **BSA** plays an active role as a support for the photosensitizer.

Photocatalytic water oxidation was studied in a system containing two ruthenium-based artificial proteins, **BSA-Ru$_{PS}$** and **BCA-Ru$_{WOC}$**, in presence of sodium persulfate as sacrificial electron acceptor (SEA). The quenching of **BSA-Ru$_{PS}$** by the SEA in solution and the formation of O_2 suggested an interaction between the two proteins may occur, as it is necessary for the oxidatively quenched **BSA-Ru$_{PS}^{+}$** species to come close enough to the catalyst **BCA-Ru$_{WOC}$** to transfer its hole there, so that the water oxidation reaction on the catalytic centre can proceed. This interaction can be supported by the fact that at low concentration of photosensitizer (20 μM), the O_2 evolution for the **BSA-Ru$_{PS}$** conjugate was higher compared to that using free $[Ru(bpy)_3]^{2+}$, indicating that the protein units, **BSA-Ru$_{PS}$** and **BCA-Ru$_{WOC}$**, interact once both in solution. This protein-protein interaction could also limit charge recombination compared with the free photosensitizer (Figure 5.9).[44,45] Furthermore, SDS-gel showed the formation of a high molecular weight species upon irradiation. Similar results were obtained when free **BSA** and **BCA** where irradiated in presence of $[Ru(bpy)_3]^{2+}$. Thus, this high-molecular weight species clearly formed only in presence of the irradiated photosensitizer-SEA mixture, suggesting that the oxidized Ru(III) trispyridyl intermediate, whether free or conjugated to **BSA**, is responsible for its formation. Regardless the presence of the photosensitizer or light, CD showed the influence of **BSA** in **BCA** conformation and vice versa, supporting protein-protein interaction. Thus, in the full photocatalytic

system protein-protein aggregation or oxidative cross-linking involving tyrosine residues, was hypothesized.[32] Moreover, in the ESI-MS deconvoluted spectrum, the signals of the initial proteins (29000 Da and 67140 Da) were not visible but signals that can be related to the oxidized species (29900 and 70380 Da). Additionally, no other signals corresponding to high-molecular weight was visible in the deconvoluted ESI-MS spectrum of the irradiated sample. DLS showed a slight increase of the size distribution in the samples after photocatalysis. These results indicated that a new species involving both proteins **BSA-Ru$_{PS}$** and **BCA-Ru$_{WOC}$** formed during the photocatalytic process. However, it is still hard at this stage to determine if this new species was due to cross-linking or aggregation.

The formation of the band at 680 nm was only observed during the light irradiation of the system in the presence of the three components (SEA, **BSA-Ru$_{PS}$** and **BCA-Ru$_{WOC}$**) indicating that there is formation of Ru^{3+}. The binding of **Ru$_{WOC}$** to the Zn^{2+} centre indicated that the complex is deeply buried into the **BCA** pocket, so that the formation of a dimeric or trimeric species while **Ru$_{WOC}$** is bound to the protein can be discarded.[46,47] The formation of this specie was achieved by electron transfer between the oxidized specie **BSA-Ru$_{PS}^{+}$** and the catalyst **BCA-Ru$_{WOC}$**, which requires a form of proximity between the two Ru centres. However, intervention of any protein residues in the electron transfer cannot be discarded. Either way, this result suggests that the proteins also need to be close enough to achieve such electron transfer (Figure 5.9)[20,48]. Time-resolved fluorescence studies showed the effect of the protein-protein interaction in emission of **Ru$_{PS}$** bound to **BSA** (Figure AIV.12). The slight changes in the lifetime when the concentration of **BCA-Ru$_{WOC}$** increased, indicates not only the change of the environment of **Ru$_{PS}$** once bound to **BSA** scaffold but give indications of a permanent interaction between proteins before light excitation (Figure 5.9). These results suggest that the interaction of the protein do not depend on the diffusion but from the affinity between them.

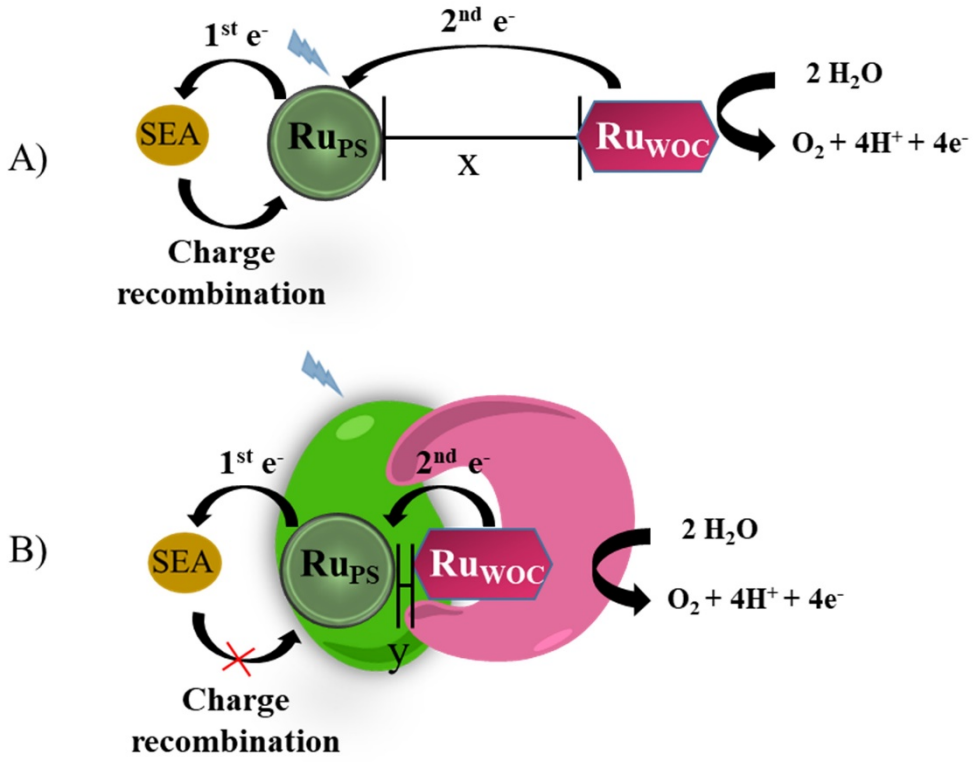

Figure 5.9. Schematic representation of the effect of the protein scaffold during photocatalytic WO reaction. (**A**) without protein scaffold and (**B**) with protein scaffold. x and y represent average distances (long *vs*. short, x > y).

5.4. Conclusion

An artificial light-harvesting protein, **BSA-Ru$_{PS}$**, was successfully prepared by covalent conjugation of a ruthenium photosensitizer *via* thiol addition of the free Cys34 of **BSA** to the maleimide group of **Ru$_{PS}$**. Then, this artificial light-harvesting protein was mixed with the **BCA-Ru$_{WOC}$** catalyst described in Chapter 4, to develop the first protein-based artificial photosystem II mimic composed of two ruthenium-based artificial metalloproteins, **BSA-Ru$_{PS}$** for photon collection and **BCA-Ru$_{WOC}$** for water oxidation catalysis. The performances of this system for O_2 evolution was good even at very low concentrations in ruthenium, suggesting that protein-protein

interaction may occur. This interaction was further studied using CD, UV-vis, time-resolved emission spectroscopies, and SDS-page gel electrophoresis. Changes in protein conformations, and the formation of new protein species after photocatalysis, were observed. In addition, the proteins showed some form of interaction in the dark also in absence of any ruthenium cofactor, indicating that a permanent protein-protein interaction is taking place that is independent from the presence of the ruthenium functional groups. More spectroscopic studies are needed to obtain detailed information on the effects of the protein scaffolds on the electron transfer rates and overall mechanism of water oxidation. However, this study paves the way towards artificial enzyme-based photocatalytic systems capable of generating solar fuels.

5.5. Experimental section

5.5.1. Synthesis of functionalized photosensitizer for protein labelling, Ru_{PS}

The compound was synthetized according to the literature.[28] $[Ru(bpy)_2Cl_2]$ (0.242 g, 0.5 mmol) and 1,10-phenanthrolin-5-amine (0.098 g, 0.500 mmol) were dissolved in a 1:1 mixture of water (5 mL) and methanol (5 mL). After 12 h refluxing under N_2 methanol was evaporated by reducing the volume to approximately 5 mL. The product precipitated from the watery solution upon further addition of KPF_6 (125 mg). The orange solid was separated by vacuum filtration and dissolved again in a small amount (4 mL) of acetonitrile/water (2:1, *v*/*v*). The solution was purified over a short column (G3 frit, inner diameter 2 cm, length 10 cm) with neutral alumina 90 (Brockmann activity I). Acetonitrile/toluene (2:1, *v*/*v*) served as the mobile phase, with an increasing percentage of acetonitrile to finally reach an acetonitrile/toluene ratio of 9:1 (*v*/*v*). The first red fraction was collected, and the solvent evaporated, to obtain 73% yield for the amino intermediate I. In a second step, the obtained intermediate I (320 mg, 0.356 mmol) and furan-2,5-dione (428 mg, 4.36 mmol) were dissolved in DMF (3 mL). The solution was stirred at room temperature in the dark for 3.5 h to promote the formation of maleic acid monoamide. $CHCl_3$ (100 mL) was

added, and the mixture was refluxed overnight at 85 °C in a Dean–Stark trap. The resulting solution was evaporated to dryness. The orange-red solid was kept in the dark and heated to 120 °C in vacuo over 5 days to obtain **Ru_{PS}**.

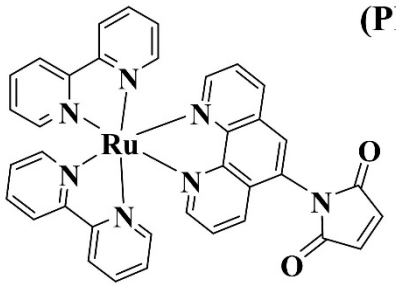

$(PF_6)_2$ **^{1}H NMR (400 MHz, MeOD)** δ 9.23 (dd, J = 8.6, 1.1 Hz, 1H), 9.03 (s, 1H), 8.79 (d, J = 8.3 Hz, 1H), 8.75 (dd, J = 8.2, 1.1 Hz, 2H), 8.60 (dd, J = 8.4, 1.2 Hz, 1H), 8.24 (dd, J = 5.2, 1.2 Hz, 1H), 8.23 – 8.16 (m, 2H), 8.13 – 8.05 (m, 3H), 7.96 (dddd, J = 5.1, 4.4, 1.5, 0.7 Hz, 2H), 7.88 (dd, J = 8.6, 5.2 Hz, 1H), 7.80 (dd, J = 8.3, 5.2 Hz, 1H), 7.67 (dd, J = 5.6, 0.7 Hz, 1H), 7.58 (dddd, J = 8.0, 5.6, 2.5, 1.3 Hz, 2H), 7.36 (dddd, J = 7.6, 5.7, 3.6, 1.3 Hz, 2H), 6.52 (d, J = 13.3 Hz, 1H), 6.20 (d, J = 13.3 Hz, 1H).**^{13}C NMR (101 MHz, MeOD)** δ 169.99, 167.04, 157.14, 152.50, 151.38, 150.98, 147.79, 145.11, 137.92, 137.55, 136.63, 134.63, 133.77, 132.18, 131.14, 130.18, 127.55, 126.61, 125.74, 124.33, 117.43, 114.87. **HRMS: $[M\text{-}2PF_6]^{2+}$** calculated mass = 344.55502, detected mass = 344.55559; **$[M\text{-}2PF_6\text{+}H_2O]^{2+}$** calculated mass = 353.56021, detected mass = 353.56046.

5.5.2. Conjugation of BSA and the photosensitizer Ru_{PS}

A solution of **BSA** from Sigma Aldrich (A7906-50G) (132 mg, 1.98 μmol) in phosphate buffer pH 7.0 (10 mL) was prepared (0.2 mM). A stock solution of **Ru_{PS}** (20 mg, 0.02 mmol) in dry DMF (1 mL, 20.4 mM) was prepared. The solution of **Ru_{PS}** was added to the solution containing the protein giving a total volume of 11 mL keeping DMF concentration lower than 10% and the sample was mixed overnight in the dark at room temperature in a closed tube. After ~12 h incubation, excess of **Ru_{PS}** was removed using a Corning concentrator (3500 MWCO. 5000 rpm, 30 min). When the solution was approximatively 2 mL (top part of concentrator), 10 mL of phosphate buffer pH 7 (20 mM) was added and the sample was re-

concentrated until ~2 mL. The concentrated solution of **BSA-Ru$_{PS}$** + excess **Ru$_{PS}$** (top part of concentrator) was purified using a Hitrap desalting column (Sigma Aldrich, 5 mL, GE17-1408-01 with phosphate buffer pH 7 (20 mM) to removes excess of **Ru$_{PS}$**. The sample was re-concentrated to a ~2 mL volume and the protein concentration was measured using a Bicinchoninic acid kit (BCA protein assay kit) from Bio-Rad (#5000116). The **BSA**:**Ru$_{PS}$** ratio was analysed by ICP-MS. Aliquots of 0.5 mL of protein solution were frozen with liquid N_2 and store in the freezer at -80 ºC for future use.

5.5.3. Lifetime emission measurements for BSA-Ru$_{PS}$

A solution of **BSA-Ru$_{PS}$** (1 mL, 10 μM) was prepared from a frozen aliquot **BSA-Ru$_{PS}$** (330 μM) which was thawed before use, and phosphate buffer pH 7.5 (80 mM). A stock solution of **BCA-Ru$_{WOC}$** (208 μM) was thawed as well. The buffer of **BCA-Ru$_{WOC}$** was exchanged to phosphate buffer pH 7.5 (80 mM) using a Corning concentrator (3500 MWCO), adding the buffer to the de-frozen solution, and centrifuging the sample until the volume reached ~1 mL. This procedure was repeated thrice. The protein concentration was measured using a BCA-kit. Samples were then degassed before use using Ar bubbling for 30 min. For each solution containing **BSA-Ru$_{PS}$** and **BCA-Ru$_{WOC}$**, the necessary volume from both protein stock solution was taken, to reach the final concentration. For emission measurements were performed with a F929 spectrometer from Edinburg instruments using a Xe900 lamp as light source and R928P emission detector. Data was recorded and processed using FS900 software. For lifetime measurements a Fluotime300 spectrometer (PicoQuant) was used, equipped with a PDL 820 Diode laser driver, a PicoHarp 300 TCSPC module/picosecond event timer and a Picosecond Laser Diode Head LDH-P-C-470. Data was processed using the software EasyTau and Fluofit.

5.6 References

(1) Fields, S.; Song, O. A Novel Genetic System to Detect Protein–Protein Interactions. *Nature* **1989**, *340* (6230), 245–246. https://doi.org/10.1038/340245a0.

(2) De Keersmaecker, H.; Camacho, R.; Rantasa, D. M.; Fron, E.; Uji-i, H.; Mizuno, H.; Rocha, S. Mapping Transient Protein Interactions at the Nanoscale in Living Mammalian Cells. *ACS Nano* **2018**, *12* (10), 9842–9854. https://doi.org/10.1021/acsnano.8b01227.

(3) Thakur, A. K.; Movileanu, L. Real-Time Measurement of Protein–Protein Interactions at Single-Molecule Resolution Using a Biological Nanopore. *Nat Biotechnol* **2019**, *37* (1), 96–101. https://doi.org/10.1038/nbt.4316.

(4) Bachmeier, A.; Murphy, B. J.; Armstrong, F. A. A Multi-Heme Flavoenzyme as a Solar Conversion Catalyst. *J. Am. Chem. Soc.* **2014**, *136* (37), 12876–12879. https://doi.org/10.1021/ja507733j.

(5) Jeuken, L. J. C.; Jones, A. K.; Chapman, S. K.; Cecchini, G.; Armstrong, F. A. Electron-Transfer Mechanisms through Biological Redox Chains in Multicenter Enzymes. *J. Am. Chem. Soc.* **2002**, *124* (20), 5702–5713. https://doi.org/10.1021/ja012638w.

(6) Yoneda, Y.; Noji, T.; Katayama, T.; Mizutani, N.; Komori, D.; Nango, M.; Miyasaka, H.; Itoh, S.; Nagasawa, Y.; Dewa, T. Extension of Light-Harvesting Ability of Photosynthetic Light-Harvesting Complex 2 (LH2) through Ultrafast Energy Transfer from Covalently Attached Artificial Chromophores. *J. Am. Chem. Soc.* **2015**, *137* (40), 13121–13129. https://doi.org/10.1021/jacs.5b08508.

(7) Pinnola, A. The Rise and Fall of Light-Harvesting Complex Stress-Related Proteins as Photoprotection Agents during Evolution. *Journal of Experimental Botany* **2019**, *70* (20), 5527–5535. https://doi.org/10.1093/jxb/erz317.

(8) Wang, C.; O'Hagan, M. P.; Willner, B.; Willner, I. Bioinspired Artificial Photosynthetic Systems. *Chemistry A European J* **2022**, *28* (9). https://doi.org/10.1002/chem.202103595.

(9) Klein, D. M.; Rodríguez-Jiménez, S.; Hoefnagel, M. E.; Pannwitz, A.; Prabhakaran, A.; Siegler, M. A.; Keyes, T. E.; Reisner, E.; Brouwer, A. M.; Bonnet, S. Shorter Alkyl Chains Enhance Molecular Diffusion and Electron Transfer Kinetics between Photosensitisers and Catalysts in CO_2 -Reducing Photocatalytic Liposomes. *Chemistry A European J* **2021**, *27* (68), 17203–17212. https://doi.org/10.1002/chem.202102989.

(10) Pannwitz, A.; Klein, D. M.; Rodríguez-Jiménez, S.; Casadevall, C.; Song, H.; Reisner, E.; Hammarström, L.; Bonnet, S. Roadmap towards Solar Fuel Synthesis at the Water Interface of Liposome Membranes. *Chem. Soc. Rev.* **2021**, *50* (8), 4833–4855. https://doi.org/10.1039/D0CS00737D.

(11) Kerns, S. A.; Biswas, A.; Minnetian, N. M.; Borovik, A. S. Artificial Metalloproteins: At the Interface between Biology and Chemistry. *JACS Au* **2022**, *2* (6), 1252–1265. https://doi.org/10.1021/jacsau.2c00102.

(12) Rapson, T. D.; Ju, H.; Marshall, P.; Devilla, R.; Jackson, C. J.; Giddey, S.; Sutherland, T. D. Engineering a Solid-State Metalloprotein Hydrogen Evolution Catalyst. *Sci Rep* **2020**, *10* (1), 3774. https://doi.org/10.1038/s41598-020-60730-y.

(13) Sommer, D. J.; Vaughn, M. D.; Ghirlanda, G. Protein Secondary-Shell Interactions Enhance the Photoinduced Hydrogen Production of Cobalt Protoporphyrin IX. *Chem. Commun.* **2014**, *50* (100), 15852–15855. https://doi.org/10.1039/C4CC06700B.

(14) Esmieu, C.; Raleiras, P.; Berggren, G. From Protein Engineering to Artificial Enzymes – Biological and Biomimetic Approaches towards Sustainable Hydrogen Production. *Sustainable Energy Fuels* **2018**, *2* (4), 724–750. https://doi.org/10.1039/C7SE00582B.

(15) Stikane, A.; Hwang, E. T.; Ainsworth, E. V.; Piper, S. E. H.; Critchley, K.; Butt, J. N.; Reisner, E.; Jeuken, L. J. C. Towards Compartmentalized Photocatalysis: Multihaem Proteins as Transmembrane Molecular Electron Conduits. *Faraday Discuss.* **2019**, *215*, 26–38. https://doi.org/10.1039/C8FD00163D.

(16) Taylor, R. J.; Geeson, M. B.; Journeaux, T.; Bernardes, G. J. L. Chemical and Enzymatic Methods for Post-Translational Protein–Protein Conjugation. *J. Am. Chem. Soc.* **2022**, *144* (32), 14404–14419. https://doi.org/10.1021/jacs.2c00129.

(17) Valtonen, S.; Vuorinen, E.; Kariniemi, T.; Eskonen, V.; Le Quesne, J.; Bushell, M.; Härmä, H.; Kopra, K. Nanomolar Protein–Protein Interaction Monitoring with a Label-Free Protein-Probe Technique. *Anal. Chem.* **2020**, *92* (24), 15781–15788. https://doi.org/10.1021/acs.analchem.0c02823.

(18) Marks, K. M.; Nolan, G. P. Chemical Labeling Strategies for Cell Biology. *Nat Methods* **2006**, *3* (8), 591–596. https://doi.org/10.1038/nmeth906.

(19) Sokol, K. P.; Robinson, W. E.; Warnan, J.; Kornienko, N.; Nowaczyk, M. M.; Ruff, A.; Zhang, J. Z.; Reisner, E. Bias-Free Photoelectrochemical Water Splitting with Photosystem II on a Dye-Sensitized Photoanode Wired to Hydrogenase. *Nat Energy* **2018**, *3* (11), 944–951. https://doi.org/10.1038/s41560-018-0232-y.

(20) McMillan, D. G. G.; Marritt, S. J.; Firer-Sherwood, M. A.; Shi, L.; Richardson, D. J.; Evans, S. D.; Elliott, S. J.; Butt, J. N.; Jeuken, L. J. C. Protein–Protein Interaction Regulates the Direction of Catalysis and Electron Transfer in a Redox Enzyme Complex. *J. Am. Chem. Soc.* **2013**, *135* (28), 10550–10556. https://doi.org/10.1021/ja405072z.

(21) Zhang, J. Z.; Reisner, E. Advancing Photosystem II Photoelectrochemistry for Semi-Artificial Photosynthesis. *Nat Rev Chem* **2020**, *4* (1), 6–21. https://doi.org/10.1038/s41570-019-0149-4.

(22) Zhang, H.; Catania, R.; Jeuken, L. J. C. Membrane Protein Modified Electrodes in Bioelectrocatalysis. *Catalysts* **2020**, *10* (12), 1427. https://doi.org/10.3390/catal10121427.

(23) Villarejo, A. A Photosystem II-Associated Carbonic Anhydrase Regulates the Efficiency of Photosynthetic Oxygen Evolution. *The EMBO Journal* **2002**, *21* (8), 1930–1938. https://doi.org/10.1093/emboj/21.8.1930.

(24) Shitov, A. V.; Terentyev, V. V.; Zharmukhamedov, S. K.; Rodionova, M. V.; Karacan, M.; Karacan, N.; Klimov, V. V.; Allakhverdiev, S. I. Is Carbonic Anhydrase Activity of Photosystem II Required for Its Maximum Electron Transport Rate? *Biochimica et Biophysica Acta (BBA) - Bioenergetics* **2018**, *1859* (4), 292–299. https://doi.org/10.1016/j.bbabio.2018.01.009.

(25) Yuan, Y.; Wang, X.; Mei, B.; Zhang, D.; Tang, A.; An, L.; He, X.; Jiang, J.; Liang, G. Labeling Thiols on Proteins, Living Cells and Tissues with Enhanced Emission Induced by FRET. *Sci Rep* **2013**, *3* (1), 3523. https://doi.org/10.1038/srep03523.

(26) Chen, X.; Wu, Y.-W. Selective Chemical Labeling of Proteins. *Org. Biomol. Chem.* **2016**, *14* (24), 5417–5439. https://doi.org/10.1039/C6OB00126B.

(27) Geng, J.; Mantovani, G.; Tao, L.; Nicolas, J.; Chen, G.; Wallis, R.; Mitchell, D. A.; Johnson, B. R. G.; Evans, S. D.; Haddleton, D. M. Site-Directed Conjugation of "Clicked" Glycopolymers To Form Glycoprotein Mimics: Binding to Mammalian Lectin and Induction of Immunological Function. *J. Am. Chem. Soc.* **2007**, *129* (49), 15156–15163. https://doi.org/10.1021/ja072999x.

(28) Terpetschnig, E.; Dattelbaum, J. D.; Szmacinski, H.; Lakowicz, J. R. Synthesis and Spectral Characterization of a Thiol-Reactive Long-Lifetime Ru(II) Complex. *Analytical Biochemistry* **1997**, *251* (2), 241–245. https://doi.org/10.1006/abio.1997.2253.

(29) Ishii, S.; Sato, S.; Asami, H.; Hasegawa, T.; Kohno, J.-Y.; Nakamura, H. Design of S–S Bond Containing Maleimide-Conjugated *Closo* -

Dodecaborate (SSMID): Identification of Unique Modification Sites on Albumin and Investigation of Intracellular Uptake. *Org. Biomol. Chem.* **2019**, *17* (22), 5496–5499. https://doi.org/10.1039/C9OB00584F.

(30) Anand, U.; Jash, C.; Boddepalli, R. K.; Shrivastava, A.; Mukherjee, S. Exploring the Mechanism of Fluorescence Quenching in Proteins Induced by Tetracycline. *J. Phys. Chem. B* **2011**, *115* (19), 6312–6320. https://doi.org/10.1021/jp2008978.

(31) Limburg, B.; Bouwman, E.; Bonnet, S. Rate and Stability of Photocatalytic Water Oxidation Using $[Ru(Bpy)_3]^{2+}$ as Photosensitizer. *ACS Catal.* **2016**, *6* (8), 5273–5284. https://doi.org/10.1021/acscatal.6b00107.

(32) Meunier, S.; Strable, E.; Finn, M. G. Crosslinking of and Coupling to Viral Capsid Proteins by Tyrosine Oxidation. *Chemistry & Biology* **2004**, *11* (3), 319–326. https://doi.org/10.1016/j.chembiol.2004.02.019.

(33) Angerani, S.; Winssinger, N. Visible Light Photoredox Catalysis Using Ruthenium Complexes in Chemical Biology. *Chem. Eur. J.* **2019**, *25* (27), 6661–6672. https://doi.org/10.1002/chem.201806024.

(34) Grądzka-Kurzaj, I.; Gierszewski, M.; Timmer, B. J. J.; Ziółek, M. Molecular Water Oxidation Catalysis: Characterization of Subnanosecond Processes and Ruthenium "Green Dimer" Formation. *ACS Appl. Energy Mater.* **2021**, *4* (3), 2440–2450. https://doi.org/10.1021/acsaem.0c02959.

(35) Polyansky, D. E.; Muckerman, J. T.; Rochford, J.; Zong, R.; Thummel, R. P.; Fujita, E. Water Oxidation by a Mononuclear Ruthenium Catalyst: Characterization of the Intermediates. *J. Am. Chem. Soc.* **2011**, *133* (37), 14649–14665. https://doi.org/10.1021/ja203249e.

(36) Akhtar, U. S.; Tae, E. L.; Chun, Y. S.; Hwang, I. C.; Yoon, K. B. Insights into Decomposition Pathways and Fate of $Ru(Bpy)_3^{2+}$ during Photocatalytic Water Oxidation with $S_2O_8^{2-}$ as Sacrificial Electron Acceptor. *ACS Catal.* **2016**, *6* (12), 8361–8369. https://doi.org/10.1021/acscatal.6b02595.

(37) Sood, D.; Kumar, N.; Rathee, G.; Singh, A.; Tomar, V.; Chandra, R. Mechanistic Interaction Study of Bromo-Noscapine with Bovine Serum Albumin Employing Spectroscopic and Chemoinformatics Approaches. *Sci Rep* **2018**, *8* (1), 16964. https://doi.org/10.1038/s41598-018-35384-6.

(38) Roy, S.; Nandi, R. K.; Ganai, S.; Majumdar, K. C.; Das, T. K. Binding Interaction of Phosphorus Heterocycles with Bovine Serum Albumin: A Biochemical Study. *Journal of Pharmaceutical Analysis* **2017**, *7* (1), 19–26. https://doi.org/10.1016/j.jpha.2016.05.009.

(39) Iikuni, S.; Okada, Y.; Shimizu, Y.; Watanabe, H.; Ono, M. Modulation of the Pharmacokinetics of a Radioligand Targeting Carbonic Anhydrase-IX with Albumin-Binding Moieties. *Mol. Pharmaceutics* **2021**, *18* (3), 966–975. https://doi.org/10.1021/acs.molpharmaceut.0c00953.

(40) Karthikeyan, S.; Yue, X.; Festa, A. A.; Voskressensky, L. G. Understanding the Binding Information of 1-Imino-1,2-Dihydropyrazino[1,2-a]Indol-3(4H)-One in Bovine Serum Albumin, 5-Hydroxytryptamine Receptor 1B and Human Carbonic Anhydrase I: A Biophysical Approach. *Journal of Molecular Liquids* **2020**, *304*, 112793. https://doi.org/10.1016/j.molliq.2020.112793.

(41) Tatiparti, K.; Sau, S.; Gawde, K.; Iyer, A. Copper-Free 'Click' Chemistry-Based Synthesis and Characterization of Carbonic Anhydrase-IX Anchored Albumin-Paclitaxel Nanoparticles for Targeting Tumor Hypoxia. *IJMS* **2018**, *19* (3), 838. https://doi.org/10.3390/ijms19030838.

(42) Zhu, W.; Liu, Y.; Yang, Z.; Zhang, L.; Xiao, L.; Liu, P.; Wang, J.; Yi, C.; Xu, Z.; Ren, J. Albumin/Sulfonamide Stabilized Iron Porphyrin Metal Organic Framework Nanocomposites: Targeting Tumor Hypoxia by Carbonic Anhydrase IX Inhibition and $T_1 - T_2$ Dual Mode MRI Guided Photodynamic/Photothermal Therapy. *J. Mater. Chem. B* **2018**, *6* (2), 265–276. https://doi.org/10.1039/C7TB02818K.

(43) Kokhan, O.; Ponomarenko, N. S.; Pokkuluri, P. R.; Schiffer, M.; Mulfort, K. L.; Tiede, David. M. Bidirectional Photoinduced Electron Transfer in Ruthenium(II)-Tris-Bipyridyl-Modified PpcA, a Multi-Heme *c* -Type Cytochrome from *Geobacter Sulfurreducens*. *J. Phys. Chem. B* **2015**, *119* (24), 7612–7624. https://doi.org/10.1021/jp511558f.

(44) Kajihara, R.; Oohora, K.; Hayashi, T. Photoinduced Electron Transfer within Supramolecular Hemoprotein Co-Assemblies and Heterodimers Containing Fe and Zn Porphyrins. *Journal of Inorganic Biochemistry* **2019**, *193*, 42–51. https://doi.org/10.1016/j.jinorgbio.2019.01.001.

(45) Natali, M.; Orlandi, M.; Berardi, S.; Campagna, S.; Bonchio, M.; Sartorel, A.; Scandola, F. Photoinduced Water Oxidation by a Tetraruthenium Polyoxometalate Catalyst: Ion-Pairing and Primary Processes with Ru(Bpy)32+ Photosensitizer. *Inorg. Chem.* **2012**, *51* (13), 7324–7331. https://doi.org/10.1021/ic300703f.

(46) Yang, Q.-Q.; Jiang, X.; Yang, B.; Wang, Y.; Tung, C.-H.; Wu, L.-Z. Amphiphilic Oxo-Bridged Ruthenium "Green Dimer" for Water Oxidation. *iScience* **2020**, *23* (3), 100969. https://doi.org/10.1016/j.isci.2020.100969.

(47) Zhang, B. Characterization of a Trinuclear Ruthenium Species in Catalytic Water Oxidation by Ru(Bda)(Pic)2 in Neutral Media. **2016**.

(48) Winkler, J. R.; Gray, H. B. Electron Flow through Metalloproteins. *Chem. Rev.* **2014**, *114* (7), 3369–3380. https://doi.org/10.1021/cr4004715.